Inverse Problems **16** (2000) 681–699. Printed in the UK PII: S0266-5611(00)09867-1

An implementation of the reconstruction algorithm of A Nachman for the 2D inverse conductivity problem

Samuli Siltanen†§, Jennifer Mueller‡ and David Isaacson‡

† Helsinki University of Technology, Espoo, Finland
‡ Rensselaer Polytechnic Institute, Troy, NY, USA

Received 25 November 1999, in final form 16 February 2000

Abstract. The 2D inverse conductivity problem requires one to determine the unknown electrical conductivity distribution inside a bounded domain $\Omega \subset \mathbb{R}^2$ from knowledge of the Dirichlet-to-Neumann map. The problem has geophysical, industrial, and medical imaging (electrical impedance tomography) applications.

In 1996 A Nachman proved that the Dirichlet-to-Neumann map uniquely determines C^2 conductivities. The proof, which is constructive, outlines a direct method for reconstructing the conductivity. In this paper we present an implementation of the algorithm in Nachman's proof. The paper includes numerical results obtained by applying the general algorithms described to two radially symmetric cases of small and large contrast.

(Some figures in this article are in colour only in the electronic version; see `www.iop.org`)

1. Introduction

Let $\Omega \subset \mathbb{R}^2$ be a bounded, simply connected C^∞ domain and $\gamma : \Omega \to \mathbb{R}$ a $C^2(\Omega)$ function with a strictly positive lower bound: $0 < c \leqslant \gamma(x)$. Furthermore, assume that $\gamma \equiv 1$ in a neighbourhood of $\partial\Omega$.

Define the Dirichlet-to-Neumann map corresponding to γ by

$$\Lambda_\gamma : H^{1/2}(\partial\Omega) \to H^{-1/2}(\partial\Omega), \qquad \langle \Lambda_\gamma f, g \rangle = \int_\Omega \gamma \nabla u \cdot \nabla v, \tag{1}$$

where v is any $H^1(\Omega)$ function with trace g on the boundary and $u \in H^1(\Omega)$ solves the Dirichlet problem

$$\begin{aligned} &\nabla \cdot \gamma \nabla u = 0 \text{ in } \Omega, \\ &u|_{\partial\Omega} = f. \end{aligned} \tag{2}$$

Equation (2) is a model for the electric potential u in a 2D bounded domain Ω with conductivity $\gamma(x)$ given the voltage f on the boundary. The quantity $\gamma \frac{\partial u}{\partial \nu}|_{\partial\Omega}$ represents the current density on the boundary. The Dirichlet-to-Neumann map is often referred to as the voltage-to-current map for the conductivity equation since, informally,

$$\Lambda_\gamma : f \mapsto \gamma \frac{\partial u}{\partial \nu}\bigg|_{\partial\Omega}.$$

The inverse conductivity problem is to determine $\gamma(x)$ from knowledge of the Dirichlet-to-Neumann map Λ_γ. The physical interpretation of Λ_γ is knowledge of the resulting current

§ Present address: Instrumentarium Corp. Imaging Division, Tuusula, Finland.

0266-5611/00/030681+19$30.00

distributions on the boundary of Ω corresponding to all possible voltage distributions on the boundary. See, for example, [27] for further discussion of the Dirichlet-to-Neumann map and results on the inverse conductivity problem in $\mathbb{R}^3$.

One application of the inverse conductivity problem is a medical imaging technique known as electrical impedance tomography (EIT). In EIT the domain Ω is often a cross section of the body, such as a patient's chest. The tissues and organs in the body have different conductivities, a fact which enables one to form an image from the conductivity distribution $\gamma(x)$. By applying a basis of current patterns on electrodes attached around the patient's chest and measuring the resulting voltages on the electrodes, the solution to the inverse conductivity problem yields a 2D image of a cross section of the chest. See [9] for further information and images made by EIT techniques and [2] or [21] for 3D images.

Motivated by geophysical applications, in 1980 Calderón [7] showed how to determine nearly constant conductivities from the Dirichlet-to-Neumann map. He posed the fundamental question: does knowledge of the Dirichlet-to-Neumann map uniquely determine the conductivity γ, and if so, is it possible to reconstruct γ? In 1985 Kohn and Vogelius [17] proved that if $\partial\Omega$ is C^∞ and γ is piecewise analytic, then Λ_γ determines γ uniquely in dimensions $n \geqslant 2$. In [26] Sylvester and Uhlmann showed that if $\partial\Omega$ is C^∞, then Λ_γ uniquely determines γ in $C^\infty(\bar{\Omega})$ in dimensions $n \geqslant 3$. Nachman gave a reconstruction method in [22] in dimensions $n \geqslant 3$ for $\gamma \in C^{1,1}$ with $\partial\Omega \in C^{1,1}$. The global uniqueness question in two-dimensions remained open until 1995, when it was resolved for $\partial\Omega$ Lipschitz and $\gamma \in W^{2,p}(\Omega)$, $p > 1$, by Nachman [23]. This result was sharpened in 1997 to $W^{1,p}(\Omega)$, $p > 2$, conductivities by Brown and Uhlmann [6]. For generalizations of the above results to more general spaces and other related work see the references given in [15, 23, 27].

We recall the main result in [23] in a form suitable for us. Let Ω be a bounded, simply connected C^∞ domain in $\mathbb{R}^2$; let γ_1 and γ_2 be in $C^2(\Omega)$ and have positive lower bounds. Then $\Lambda_{\gamma_1} = \Lambda_{\gamma_2}$ implies $\gamma_1 = \gamma_2$. It is an important feature of Nachman's proof that it gives a constructive procedure for recovering γ from knowledge of Λ_γ. It is the purpose of this paper to provide the first implementation of that procedure. The algorithm is a direct method based on the techniques of inverse scattering. It does not rely on the minimization of a cost functional or on iteration. For a survey of other reconstruction algorithms, see [8] or [28]; note also [4, 5, 16] and the references in [9]. Due to the nature of the algorithm, which requires a number of definitions, a description of Nachman's algorithm is reserved for section 2.

The paper is organized as follows. In section 2 we describe the reconstruction algorithm outlined in Nachman's proof. Section 3 contains new theoretical results relevant to the numerical implementation. In section 4 we describe our method of implementation of the solution to various aspects of the forward problem. We provide a method for numerically computing the Faddeev Green function. For given γ, we describe a method of constructing the Dirichlet-to-Neumann map, Faddeev exponential solutions and an intermediate object known as the non-physical scattering transform $\boldsymbol{t}(k)$. The results are used to check our intermediate computations. Section 5 contains the implementation of steps in the algorithm related to the solution of the inverse problem. Here we describe how the numerical approximation to $\boldsymbol{t}(k)$ is obtained from the Dirichlet-to-Neumann map Λ_γ and describe a method for the solution to the $\bar{\partial}$-equation containing $\boldsymbol{t}(k)$. Section 6 contains examples of the complete method applied to the reconstruction of two infinitely smooth rotationally symmetric conductivity distributions of small and large contrast. This class of examples was chosen because it permits a very accurate representation for Λ_γ (see section 4.1) and simplifies the computation of $\boldsymbol{t}(k)$ (see section 5.1).

Throughout the paper we identify planar points $x = (x_1, x_2)$ with the corresponding complex number $x = x_1 + \mathrm{i}x_2$; the product kx always denotes complex multiplication.

2. Outline of the method

The unknown coefficient can be removed from the higher-order terms in the conductivity equation by transforming (1) to the Schrödinger equation as follows. Let $q \in C_0^0(\Omega)$ be given by $q = \gamma^{-1/2}\Delta\gamma^{1/2}$. If u is a solution of $\nabla \cdot \gamma\nabla u = 0$ in Ω, defining $\tilde{u} = \gamma^{1/2}u$ yields

$$(-\Delta + q)\tilde{u} = 0 \qquad \text{in} \quad \Omega. \tag{3}$$

Our assumption that γ be one near $\partial\Omega$ allows us to smoothly extend $\gamma = 1$ and $q = 0$ to the whole plane. We may therefore study equation (3) in all of $\mathbb{R}^2$.

The exponentially behaving solutions of (3) introduced by Faddeev [11] are the key to the reconstruction. By theorem 1.1 of [23] for any $k \in \mathbb{C} \setminus 0$ there is a unique solution $\psi(x, k)$ of

$$(-\Delta + q)\psi(x, k) = 0 \qquad \text{in} \quad \mathbb{R}^2 \tag{4}$$

satisfying $e^{-ikx}\psi(\cdot, k) - 1 \in W^{1,\tilde{p}}$ for any $2 < \tilde{p} < \infty$. The space $W^{1,\tilde{p}} = W^{1,\tilde{p}}(\mathbb{R}^2)$ is a special case of the definition

$$W^{m,\rho}(E) = \{f \in L^\rho(E) | \partial^\alpha f \in L^\rho(E), |\alpha| \leqslant m\}$$

for an arbitrary domain $E \subset \mathbb{R}^n$ and $1 \leqslant \rho \leqslant \infty, m \geqslant 0$. Denote

$$\mu(x, k) := e^{-ikx}\psi(x, k), \qquad x \in \mathbb{R}^2, \qquad k \in \mathbb{C} \setminus 0, \tag{5}$$

and note that the condition $\mu - 1 \in W^{1,\tilde{p}}$ and the Sobolev imbedding theorem yield that μ is continuous and tends to one asymptotically when $|x| \to \infty$.

The reconstruction of γ is based on the use of an intermediate object called the *non-physical scattering transform* $\boldsymbol{t}$, which is not directly measurable in experiments:

$$\boldsymbol{t}(k) := \int_{\mathbb{R}^2} e_k(x)\mu(x, k)q(x)\,dx, \qquad k \in \mathbb{C} \setminus 0, \tag{6}$$

where $e_k(x) := \exp(i(kx + \bar{k}\bar{x}))$. Note that since μ is asymptotically close to one, $\boldsymbol{t}(k)$ is approximately the Fourier transform of $q(x)$ evaluated at the point $(-2k_1, 2k_2) \in \mathbb{R}^2$. We explain the two main steps of the method, namely finding $\boldsymbol{t}$ from Λ_γ and determining γ from the knowledge of $\boldsymbol{t}$.

Define a single-layer operator S_k for $k \in \mathbb{C} \setminus 0$ by

$$(S_k\phi)(x) := \int_{\partial\Omega} G_k(x - y)\phi(y)\,d\sigma(y), \tag{7}$$

where $G_k(x)$ is the Faddeev Green function

$$G_k(x) := e^{ikx}g_k(x), \qquad -\Delta G_k = \delta, \tag{8}$$

$$g_k(x) := \frac{1}{(2\pi)^2}\int_{\mathbb{R}^2} \frac{e^{ix\cdot\xi}}{\xi(\bar{\xi} + 2k)}d\xi, \qquad (-\Delta - 4ik\bar{\partial})g_k = \delta, \tag{9}$$

where $\bar{\partial} = (\partial/\partial x_1 + i\partial/\partial x_2)/2$ and $x \cdot \xi = x_1\xi_1 + x_2\xi_2$; in the denominator we have $\xi = \xi_1 + i\xi_2$ and complex multiplication.

Denote the Dirichlet-to-Neumann map of the homogeneous conductivity 1 by Λ_1 and note that since $\gamma \equiv 1$ near $\partial\Omega$ the maps Λ_γ and the Dirichlet-to-Neumann map Λ_q of the Schrödinger problem are the same. By theorem 5 of [23] the trace on $\partial\Omega$ of the function $\psi(\cdot, k)$ satisfies the integral equation

$$\psi(\cdot, k)|_{\partial\Omega} = e^{ikx} - S_k(\Lambda_\gamma - \Lambda_1)\psi(\cdot, k) \tag{10}$$

for any $k \in \mathbb{C} \setminus 0$. The operator $I + S_k(\Lambda_\gamma - \Lambda_1)$ is invertible on $H^{1/2}(\partial\Omega)$, so we can solve (10). Furthermore, if $\psi(\cdot, k)|_{\partial\Omega}$ has been determined, then $\boldsymbol{t}(k)$ can be recovered from the formula

$$\boldsymbol{t}(k) = \int_{\partial\Omega} e^{i\bar{k}\bar{x}}(\Lambda_\gamma - \Lambda_1)\psi(\cdot, k)\,d\sigma. \tag{11}$$

The non-physical scattering transform contains enough information to recover γ. Namely, theorem 2.1 of [23] implies that the $\bar\partial$ equation

$$\frac{\partial}{\partial\bar k}\mu(x,k)=\frac{1}{4\pi\bar k}\boldsymbol{t}(k)e_{-k}(x)\overline{\mu(x,k)},\qquad k\neq 0, \tag{12}$$

holds and theorem 4.1 of [23] shows that (12) is uniquely solvable. The solution satisfies

$$\mu(x,k)=1+\frac{1}{(2\pi)^2}\int_{\mathbb{R}^2}\frac{\boldsymbol{t}(k')}{(k-k')\bar{k'}}e_{-x}(k')\overline{\mu(x,k')}\,\mathrm{d}k'_1\mathrm{d}k'_2 \tag{13}$$

for all $k\in\mathbb{C}\setminus 0$, $x\in\mathbb{R}^2$. Note that the integral is taken over the k-plane, so to solve (13), $\mu(x,k)$ is needed for all values of $k\in\mathbb{C}\setminus 0$. The functions $\mu(x,k)$ can be used to recover γ [23, section 3]:

$$\gamma^{1/2}(x)=\lim_{k\to 0}\mu(x,k). \tag{14}$$

Note that in the solution of the $\bar\partial$ equation x is kept fixed, so the computations can be carried out only in the region of interest.

In summary, the main steps of the algorithm of A Nachman are:

(1) Compute the trace on $\partial\Omega$ of the function $\psi(\cdot,k)$ from the boundary data using equation (10).
(2) Compute the scattering transform $\boldsymbol{t}(k)$ using equation (11).
(3) Compute $\mu(x,k)$ by using (13) to solve the $\bar\partial$ equation (12).
(4) Reconstruct $\gamma(x)$ using equation (14).

We remark that in [23] the first step in Nachman's scheme is finding $\gamma|_{\partial\Omega}$ and $\partial\gamma/\partial\nu|_{\partial\Omega}$ and continuing γ artificially to be one outside a neighbourhood of Ω. We omit that step in this implementation and consider only conductivities that are one in a neighbourhood of $\partial\Omega$.

3. Theoretical results

In the numerical solution of the $\bar\partial$ equation (12) it is crucial to understand the large and small $|k|$ behaviour of the continuous function $\boldsymbol{t}(k)$; we give an analysis in theorems 3.1 and 3.2. Moreover, any concrete knowledge on relations between properties of γ and $\boldsymbol{t}(k)$ helps in the reconstruction; it is also useful in producing test examples and testing numerical procedures. Theorem 3.3 describes equivalent properties of γ and $\boldsymbol{t}(k)$.

We start by presenting facts about the Faddeev Green functions. Let G_k and g_k be given by (8) and set $G_0:=-(2\pi)^{-1}\log|x|$. Denote

$$H_k(x):=G_k(x)-G_0(x),\qquad k\in\mathbb{C}\setminus 0. \tag{15}$$

Now, $\Delta H_k=-\delta+\delta=0$ and by Weyl's lemma $H_k(x)$ is smooth and harmonic in $\mathbb{R}^2$. Changes of variables in the integral in (9) show that g_k satisfies

$$g_k(x)=g_1(kx)=\overline{g_{\bar k}(-\bar x)}=e_{-k}(x)\overline{g_k(x)} \tag{16}$$

for $x\in\mathbb{R}^2\setminus 0$ and $k\in\mathbb{C}\setminus 0$. We see immediately that $G_k(x)=G_1(kx)$ and

$$H_k(x)=H_1(kx)-(2\pi)^{-1}\log|k|. \tag{17}$$

Furthermore, (16) yields $\overline{G_k(x)}=\mathrm{e}^{-\mathrm{i}\bar k\bar x}\overline{g_k(x)}=\mathrm{e}^{-\mathrm{i}\bar k\bar x}e_k(x)g_k(x)=\mathrm{e}^{\mathrm{i}kx}g_k(x)=G_k(x)$, so G_k (and consequently H_k) is real-valued. Since $\xi^{-1}(\bar\xi+2)^{-1}\in L^{\tilde p'}$ for all $1<\tilde p'<2$ we know from the Riesz–Thorin interpolation theorem that the inverse Fourier transform $g_1(x)=\mathcal{F}^{-1}(\xi^{-1}(\bar\xi+2)^{-1})$ belongs to $L^{\tilde p}$. Thus by (16) for all $k\in\mathbb{C}\setminus 0$ we have

$$\|g_k\|_{L^{\tilde p}}=|k|^{-2/\tilde p}\|g_1\|_{L^{\tilde p}}<\infty\qquad\text{for any}\quad 2<\tilde p<\infty. \tag{18}$$

We now move on to prove numerically significant properties of $\boldsymbol{t}$ and μ.

Theorem 3.1. *Let $\Omega \subset \mathbb{R}^2$ be a bounded, simply connected C^∞ domain. Let $\gamma \in C^2(\Omega)$ have a positive lower bound and assume $\gamma \equiv 1$ near $\partial\Omega$. With $\boldsymbol{t}(k)$ given by (6) and k close to zero we have*

$$|\boldsymbol{t}(k)| \leqslant C|k|^2, \tag{19}$$

$$|\mu(x,k) - \sqrt{\gamma(x)}| \leqslant C|k| \qquad \text{for all} \quad x \in \overline{\Omega}. \tag{20}$$

Proof. We have $(\Lambda_\gamma - \Lambda_1)1 = 0$ and $\int_{\partial\Omega} \Lambda_\gamma f = \int_{\partial\Omega} \gamma \frac{\partial u}{\partial \nu} = \int_\Omega \nabla \cdot \gamma \nabla u = 0$ for any $f \in H^{1/2}(\partial\Omega)$. The same obviously holds for Λ_1.

Let us analyse the operator $I + S_k(\Lambda_\gamma - \Lambda_1)$. Write $G_k = H_k + G_0$ and define $\tilde{H}_1(x) := H_1(x) - H_1(0)$. Apply equation (17) to get

$$I + S_k(\Lambda_\gamma - \Lambda_1) = I + S_0(\Lambda_\gamma - \Lambda_1) + \mathcal{H}_k(\Lambda_\gamma - \Lambda_1) =: A_\gamma + \mathcal{H}_k(\Lambda_\gamma - \Lambda_1), \tag{21}$$

where

$$(\mathcal{H}_k\phi)(x) = \int_{\partial\Omega} \tilde{H}_1(k(x-y))\phi(y)\,\mathrm{d}\sigma(y); \tag{22}$$

this eliminates the $\log|k|$ term in (17). We will show that A_γ is invertible in $H^{1/2}(\partial\Omega)$ and that

$$\|\mathcal{H}_k\|_{L(H^{1/2}(\partial\Omega))} \leqslant C|k| \qquad \text{for} \quad \text{small } |k|. \tag{23}$$

Denote by $R_\gamma : \tilde{H}^{-1/2}(\partial\Omega) \to \tilde{H}^{1/2}(\partial\Omega)$ the Neumann-to-Dirichlet map of γ, where $\tilde{H}^s$ spaces consist of H^s functions with mean value zero. By jump relations $R_1 = S_0$, see [10]. Setting $P\phi := |\partial\Omega|^{-1}\int_{\partial\Omega}\phi$ we find $P\Lambda_\gamma = 0$ and $R_\gamma\Lambda_\gamma = I - P$; this is true also with γ replaced by 1. It follows that

$$A_\gamma^{-1} = (S_0\Lambda_\gamma + P)^{-1} = R_\gamma\Lambda_1 + P. \tag{24}$$

To show (23), note that $\tilde{H}_1$ is smooth and vanishes at the origin. Thus for $\phi \in C_0^\infty(\partial\Omega)$ and k near zero

$$\|\mathcal{H}_k\phi\|_{L^2(\partial\Omega)} \leqslant \sup_{x,y\in\partial\Omega} |\tilde{H}_1(k(x-y))|\,\|\phi\|_{L^2(\partial\Omega)} \leqslant C|k|\|\phi\|_{L^2(\partial\Omega)},$$

$$\|(\mathcal{H}_k\phi)'\|_{L^2(\partial\Omega)} \leqslant C|k|\|\nabla\tilde{H}\|_{L^\infty(B(0,1))}\|\phi\|_{L^2(\partial\Omega)}.$$

Thus $\|\mathcal{H}_k\|_{L(H^s(\partial\Omega))} \leqslant C|k|$ for $s = 0, 1$ and (23) follows by interpolation.

By (24) we have $A_\gamma^{-1}1 = 1$. Compute for small $|k|$ with (10) and (21)

$$\begin{aligned}\psi(x,k) &= (I + S_k(\Lambda_\gamma - \Lambda_1))^{-1}\mathrm{e}^{\mathrm{i}kx} \\ &= 1 + A_\gamma^{-1}(\mathrm{e}^{\mathrm{i}kx} - 1) - A_\gamma^{-1}\mathcal{H}_k A_\gamma^{-1}\mathrm{e}^{\mathrm{i}kx} + \mathcal{O}(\mathcal{H}_k^2)\mathrm{e}^{\mathrm{i}kx}.\end{aligned}$$

For k near zero we have $\|\mathrm{e}^{\mathrm{i}kx} - 1\|_{L^2(\partial\Omega)} \leqslant C|k|$ and $\|(\mathrm{e}^{\mathrm{i}kx})'\|_{L^\infty(\partial\Omega)} \leqslant C|k|$. Hence $\|\mathrm{e}^{\mathrm{i}kx}\|_{H^{1/2}(\partial\Omega)} \leqslant C$ and $\|\mathrm{e}^{\mathrm{i}kx} - 1\|_{H^{1/2}(\partial\Omega)} \leqslant C|k|$ for small $|k|$. Now, using (23) we get

$$\|\psi(x,k) - 1\|_{H^{1/2}(\partial\Omega)} \leqslant C|k| \qquad \text{for} \quad \text{small } |k|. \tag{25}$$

Since $\gamma^{-1/2}\psi$ solves the conductivity equation in Ω, from the generalized maximum principle [12] combined with regularity and imbedding theorems we get the estimate $|\gamma^{-1/2}(x)\psi(x,k) - 1| \leqslant C|k|$ for all $x \in \overline{\Omega}$. Since $\mu(x,k) = \mathrm{e}^{-\mathrm{i}kx}\psi(x,k)$, (20) follows. To show (19), write

$$\begin{aligned}|\boldsymbol{t}(k)| &= \left|\int_{\partial\Omega} (\mathrm{e}^{\mathrm{i}\bar{k}\bar{x}} - 1)(\Lambda_\gamma - \Lambda_1)(\psi(\cdot,k) - 1)\right| \\ &\leqslant C\|\mathrm{e}^{\mathrm{i}\bar{k}\bar{x}} - 1\|_{H^{1/2}(\partial\Omega)}\|\psi(\cdot,k) - 1\|_{H^{1/2}(\partial\Omega)},\end{aligned}$$

where C is the operator norm of $\Lambda_\gamma - \Lambda_1$ from $H^{1/2}(\partial\Omega)$ to $H^{-1/2}(\partial\Omega)$. □

Theorem 3.2. *Let $\Omega \subset \mathbb{R}^2$ be a bounded, simply connected C^∞ domain. Let $\gamma \in C^{2+m}(\Omega), m \geqslant 1$, have a positive lower bound and assume $\gamma \equiv 1$ near $\partial\Omega$. Define $q = \gamma^{-1/2}\Delta\gamma^{1/2}$ and let $\boldsymbol{t}(k)$ be given by (6). Then*

$$|\boldsymbol{t}(k)| \leqslant C|k|^{-m} \qquad \text{for} \quad \text{large } |k|. \tag{26}$$

Proof. Fix $1 < p < 2$ and note that $\gamma \in W^{2,p}(\Omega)$. For all $k \in \mathbb{C} \setminus 0$ let $\mu(x, k)$ be the unique solution of $(-\Delta - 4\mathrm{i}k\bar{\partial} + q)\mu(x, k) = 0$ with $\mu - 1 \in W^{1,\tilde{p}}$ and $1/\tilde{p} := 1/p - \frac{1}{2}$; this is equivalent to (4). Recall from [23, p 82] the formula

$$\mu = 1 - [I + g_k * (q\cdot)]^{-1}(g_k * q) \tag{27}$$

valid in $W^{1,\tilde{p}}$. We will show that $\mu - 1 \in W^{m,\tilde{p}}$ and satisfies

$$\|\mu(\cdot, k) - 1\|_{W^{m,\tilde{p}}} \leqslant C|k|^{-2/\tilde{p}}\|q\|_{W^{m,1}} \qquad \text{for} \quad \text{large } |k|. \tag{28}$$

First we prove the invertibility of the operator $I + g_k * (q\cdot)$ in $W^{m,\tilde{p}}$. By [23, theorem 1.1] we know this for $m = 1$, and in particular we have injectivity $W^{m,\tilde{p}} \to W^{1,\tilde{p}}$. The inequalities of Young and Hölder together with (18) imply for any multi-indices β, β' with $|\beta|+|\beta'| = j \leqslant m$

$$\begin{aligned}\|g_k * ((\partial^\beta q)(\partial^{\beta'} f))\|_{L^{\tilde{p}}} &\leqslant \|g_k\|_{L^{\tilde{p}}}\|(\partial^\beta q)(\partial^{\beta'} f)\|_{L^1} \\ &\leqslant \|g_k\|_{L^{\tilde{p}}}\|\partial^\beta q\|_{L^{\tilde{p}'}}\|\partial^{\beta'} f\|_{L^{\tilde{p}}} \\ &\leqslant C|k|^{-2/\tilde{p}'}\|q\|_{W^{m,\tilde{p}'}}\|f\|_{W^{m,\tilde{p}}},\end{aligned} \tag{29}$$

so the restriction of $I + g_k * (q\cdot)$ to $W^{m,\tilde{p}}$ has $W^{m,\tilde{p}}$ as target space. Compactness of $g_k * (q\cdot)$ is evident from the decomposition $W^{m,\tilde{p}} \xrightarrow{\iota} C^{m-1} \xrightarrow{q\cdot} W^{m-1,p} \xrightarrow{g_k*} W^{m,\tilde{p}}$, where we used Sobolev imbedding and [23, lemma 1.3]. Invertibility now follows by a Fredholm argument.

Formula (29) shows that $\|g_k * (q\cdot)\|_{L(W^{m,\tilde{p}})} \leqslant \frac{1}{2}$ for large enough $|k|$, so

$$\|[I + g_k * (q\cdot)]^{-1}\|_{W^{m,\tilde{p}} \to W^{m,\tilde{p}}} \leqslant 2 \qquad \text{for} \quad \text{large } |k|. \tag{30}$$

An application of Young's inequality and (18) gives

$$\|g_k * q\|_{W^{m,\tilde{p}}} = \sum_{|\alpha| \leqslant m} \|g_k * (\partial^\alpha q)\|_{L^{\tilde{p}}} \leqslant C|k|^{-2/\tilde{p}'}\|q\|_{W^{m,1}}. \tag{31}$$

Substituting (30) and (31) into (27) yields (28).

To prove (26) it is enough to show that $|k_j^m \boldsymbol{t}(k)| \leqslant C(m, |\Omega|, \|q\|_{C_0^m})$ for $j = 1, 2$ and $|k|$ large enough. Write $q\mu = q(\mu - 1) + q$ in (6) and integrate by parts to get

$$|k_j^m \boldsymbol{t}(k)| \leqslant C\int_{\mathbb{R}^2} \left|\frac{\partial^m q}{\partial x_j^m}\right| \mathrm{d}x + C\int_{\mathbb{R}^2} \left|\frac{\partial^m}{\partial x_j^m}((\mu - 1)q)\right| \mathrm{d}x. \tag{32}$$

We can bound the first term of (32) by $C|\Omega| \sup_{x\in\Omega} |\partial^m q(x)/\partial x_j^m|$. For large enough $|k|$ by (28) the second integral in (32) is bounded by

$$C\|\mu(\cdot, k) - 1\|_{W^{m,\tilde{p}}}\|q\|_{W^{m,\tilde{p}'}} \leqslant C\|q\|_{W^{m,1}}\|q\|_{W^{m,\tilde{p}'}} \leqslant C|\Omega|^{1+1/\tilde{p}'}\|q\|_{C_0^m}^2.$$

□

Theorem 3.3. *Let $\gamma_i \in C^2(\mathbb{R}^2)$ have a positive lower bound and assume that $\gamma_i - 1$ is compactly supported for $i = 1, 2$. Set $q_i = \gamma_i^{-1/2}\Delta\gamma_i^{1/2}$ and denote by $\boldsymbol{t}_i$ the non-physical scattering transforms corresponding to q_i.*

Let $\varphi \in \mathbb{R}$, $\lambda > 0$ and $x' \in \mathbb{R}^2$; denote $z_\varphi := \mathrm{e}^{\mathrm{i}\varphi}(z_1 + \mathrm{i}z_2)$ for any $z \in \mathbb{R}^2$. Then each of the following four equivalences holds:

$$\begin{aligned}
&(i) \quad \gamma_2(x) = \gamma_1(x_{-\varphi}) \quad \forall x \in \mathbb{R}^2 \Leftrightarrow \boldsymbol{t}_2(k) = \boldsymbol{t}_1(k_\varphi) \quad \forall k \in \mathbb{C};\\
&(ii) \quad \gamma_2(x) = \gamma_1(\lambda x) \quad \forall x \in \mathbb{R}^2 \Leftrightarrow \boldsymbol{t}_2(k) = \boldsymbol{t}_1(\lambda^{-1}k) \quad \forall k \in \mathbb{C};\\
&(iii) \quad \gamma_2(x) = \gamma_1(-\bar{x}) \quad \forall x \in \mathbb{R}^2 \Leftrightarrow \boldsymbol{t}_2(k) = \overline{\boldsymbol{t}_1(\bar{k})} \quad \forall k \in \mathbb{C};\\
&(iv) \quad \gamma_2(x) = \gamma_1(x - x') \quad \forall x \in \mathbb{R}^2 \Leftrightarrow \boldsymbol{t}_2(k) = e_k(x')\boldsymbol{t}_1(k) \quad \forall k \in \mathbb{C}.
\end{aligned}$$

Proof. Assume that $\gamma_1(x_{-\varphi}) = \gamma_2(x)$ and note that this implies $q_1(x_{-\varphi}) = q_2(x)$. We know from (16) that $g_{k_\varphi}(x) = g_k(x_\varphi)$ and we can compute

$$(g_{k_\varphi} * q_1)(x) = \int_{\mathbb{R}^2} g_k(x_\varphi - y_\varphi) q_1(y)\,\mathrm{d}y = \rho_\varphi(g_k * q_2)(x),$$

where ρ_φ is the operator defined by $\rho_\varphi \psi(x) := \psi(x_\varphi)$. Similarly,

$$(g_{k_\varphi} * (q_1\psi))(x) = \rho_\varphi(g_k * (q_2\cdot))\rho_{-\varphi}\psi(x).$$

Noting that $\rho_\varphi^{-1} = \rho_{-\varphi}$, with (27) we compute

$$\begin{aligned}\mu_1(x, k_\varphi) &= 1 - [I + g_{k_\varphi} * (q_1\cdot\,)]^{-1}(g_{k_\varphi} * q_1)\\ &= 1 - \rho_\varphi[I + g_k * (q_2\cdot\,)]^{-1}\rho_{-\varphi}\rho_\varphi(g_k * q_2) = \mu_2(x_\varphi, k).\end{aligned}$$

Now, (6) yields $\boldsymbol{t}_1(k_\varphi) = \boldsymbol{t}_2(k)$, and sufficiency for (i) is proved. For necessity assume $\boldsymbol{t}_1(k_\varphi) = \boldsymbol{t}_2(k)$. Let $\gamma_3(x) = \gamma_1(x_{-\varphi})$ and denote by $\boldsymbol{t}_3(k)$ the scattering transform of γ_3. As a consequence of the above we know that $\boldsymbol{t}_3(k) = \boldsymbol{t}_1(k_\varphi) = \boldsymbol{t}_2(k)$ and by the uniqueness of Nachman's method $\gamma_2(x) = \gamma_3(x) = \gamma_1(x_{-\varphi})$.

The cases (ii), (iii) and (iv) can be proved similarly to case (i). □

4. The forward problem

To better understand the problem at hand and obtain numerical examples for comparison with our reconstruction, we present numerical algorithms for the forward problem of finding $\mu(x, k)$, $\boldsymbol{t}(k)$ and Λ_γ for given test conductivities.

4.1. The Dirichlet-to-Neumann map

We will take Ω to be the unit disc in our examples and express functions defined on the boundary $\partial\Omega$ in the trigonometric basis

$$\phi_n(\theta) := (2\pi)^{-1/2}\mathrm{e}^{\mathrm{i}n\theta}, \qquad n \in \mathbb{Z}. \tag{33}$$

We present a numerical method for finding a representation for Λ_γ in the above basis for radial conductivities.

If $\gamma(x) = \gamma(|x|)$ we know from [25] that the functions ϕ_n are eigenfunctions for the Dirichlet-to-Neumann maps:

$$\Lambda_\gamma\phi_n = \lambda_n\phi_n, \qquad \Lambda_1\phi_n = |n|\phi_n, \tag{34}$$

where the latter identity follows from $\Delta z^n = 0$, $z^n|_{\partial\Omega} = \sqrt{2\pi}\phi_n$. Below we compute numerical eigenvalues for Dirichlet-to Neumann maps of piecewise constant radial conductivities. If two conductivities γ_L, γ_U satisfy pointwise $\gamma_L(x) \leqslant \gamma_U(x)$, we have $\lambda_n^L \leqslant \lambda_n^U$ for the corresponding eigenvalues [13]. Approximating a continuous conductivity γ from above and below yields numerical upper and lower bounds for the eigenvalues of Λ_γ.

Lemma 4.1. *Let $\Omega \subset \mathbb{R}^2$ be the unit disc and $0 = r_0 < r_1 < \cdots < r_{N-1} < r_N = 1$, where $N \geqslant 2$. Let γ_j, $j = 1, \ldots, N$, be a collection of positive real numbers satisfying $\gamma_j \neq \gamma_{j+1}$ for $j = 1, \ldots, N-1$, and assume $\gamma_N = 1$. Set $\gamma(r) := \gamma_j$ for $r_{j-1} \leqslant r < r_j$, $j = 1, \ldots, N$.*

Then, the eigenvalues of Λ_γ are

$$\lambda_n = |n| - 2|n|(1 + C_{N-1})^{-1}, \tag{35}$$

where the numbers C_j are given recursively by $C_1 = \rho_1 r_1^{-2|n|}$ and $C_j = (\rho_j C_{j-1} + r_j^{-2|n|})/(\rho_j + C_{j-1}r_j^{2|n|})$ for $j = 2, \ldots, N-1$, where $\rho_j = (\gamma_{j+1} + \gamma_j)/(\gamma_{j+1} - \gamma_j)$.

Proof. It is immediate that $\lambda_0 = 0$, so fix $n \neq 0$. We will construct a H^1 function u_n that solves $\nabla \cdot \gamma \nabla u_n = 0$ in Ω, $u_n|_{r=1} = \phi_n$.

Write $u_n = v_n(r)\mathrm{e}^{\mathrm{i}n\theta}$ and $v_n(r) = a_j r^{|n|} + b_j r^{-|n|}$ for $r_{j-1} \leqslant r < r_j$, $j = 1, \ldots, N$. Set $b_1 = 0$, so u_n is harmonic in the innermost disc. Matching the limits $v_n(r_j^-) = v_n(r_j^+)$ and $\gamma_j \partial v_n(r_j^-)/\partial r = \gamma_{j+1} \partial v_n(r_j^+)/\partial r$ on each radius leads to $a_j = C_{j-1} b_j$ for $j = 2, \ldots, N$. On the outmost radius we get from the Dirichlet boundary value $a_N + b_N = 1/\sqrt{2\pi}$.

It is easily checked using the Green formula that the function u_n thus constructed is in $H^1(\Omega)$ and satisfies $\nabla \cdot \gamma \nabla u_n = 0$ in Ω in the weak sense. Finally, $\partial u_n/\partial r|_{r=1} = |n|(a_N - b_N)\phi_n$, so $\lambda_n = |n|(1 - 2b_N)$ and $b_N = (1 + C_{N-1})^{-1}$, and the lemma is proved. □

Note that in practice it is difficult to compute the eigenvalues of the Dirichlet-to-Neumann map accurately enough: since $\gamma \equiv 1$ near $\partial\Omega$, the eigenvalues are of the form $\lambda_n = |n| + \varepsilon$ with ε exponentially small. This problem becomes even more pronounced in the case of non-radially symmetric conductivities.

4.2. Computation of the Green function g_k

We describe a numerical algorithm for $g_k(x)$ with fixed $k \in \mathbb{C} \setminus 0$ and x ranging in $\mathbb{R}^2 \setminus 0$. Formula (16) implies that it is enough to compute g_1 and, moreover, that $g_1(x) = \overline{g_1(-\bar{x})}$. Thus knowing the values $g_1(x)$ for $x \neq 0$, $x_1 \geqslant 0$ gives g_k.

Since g_1 is singular at $x = 0$ we have to be careful near the origin. Provided we have an algorithm for g_1 with x on the unit circle, we can first compute $H_1(x) = \mathrm{e}^{\mathrm{i}x} g_1(x)$, where H_1 is the harmonic function given by (15). Then we can use the Poisson kernel to evaluate $H_1(x)$ inside the disc and write

$$g_1(x) = \mathrm{e}^{-\mathrm{i}x} H_1(x) - \frac{\mathrm{e}^{-\mathrm{i}x}}{2\pi} \log|x|, \tag{36}$$

where the singularity is explicit since H_1 is smooth.

To find a numerically feasible formula for $g_1(x)$ with $x_1 > 0$, write $\xi(\bar{\xi} + 2) = (\xi_1 + 1)^2 + (\xi_2 + \mathrm{i})^2$ and use residue calculus to get

$$g_1(x) = \frac{\mathrm{e}^{-\mathrm{i}x_1}}{2\pi} \mathrm{Re}\left[\mathrm{e}^{\mathrm{i}x_1} \int_0^\infty \frac{\mathrm{e}^{-t(x_1 + \mathrm{i}x_2)}}{t - \mathrm{i}} \, \mathrm{d}t \right]. \tag{37}$$

Compare with [3, formula (3.10)]. If needed, integration by parts gives a more rapidly decaying integrand.

The integral appearing in formula (37) can be easily modified to give better convergence properties for small x_1, too. Namely, a residue trick (different one for the cases $x_2 > 0$ and $x_2 < 0$) can be used to interchange the roles of x_1 and x_2 in (37); the resulting integral is also absolutely convergent for $x_2 \neq 0$, $x_1 \geqslant 0$. Finally, to compute $g_1(x)$ we divide the plane into suitable pieces and use the best formula in each piece [24].

4.3. Numerical solution of the Lippmann–Schwinger equation

In this section we describe a projection method for finding $\mu(\cdot, k)$ on an open square D satisfying $\mathrm{supp}(q) \subset D$. The computed values of μ can then be used to check the computations of μ from the $\bar{\partial}$ equation (section 5.2) and to compute $\boldsymbol{t}(k)$ from the scattering transform (6) to check the computations of $\boldsymbol{t}(k)$ from the Dirichlet-to-Neumann map (section 5.1).

The projection method relies on the following theorem.

Theorem 4.2. *Let $\Omega \subset \mathbb{R}^2$ be a bounded, simply connected C^∞ domain. Let $\gamma \in C^\infty(\Omega)$ have a positive lower bound and assume $\gamma \equiv 1$ near $\partial\Omega$. Set $q = \gamma^{-1/2} \Delta \gamma^{1/2}$ and extend*

q by zero to $\mathbb{R}^2$. For any $k \in \mathbb{C} \setminus 0$ denote by $\mu(x,k)$ the unique smooth solution of $(-\Delta - 4ik\bar{\partial} + q)\mu(\cdot,k) = 0$ satisfying $\mu(\cdot,k) - 1 \in W^{1,\tilde{p}}$ for some $2 < \tilde{p} < \infty$.

Take any bounded domain $D \subset \mathbb{R}^2$ with $\operatorname{supp}(q) \subset D$. *Then the operator*

$$I + g_k * (q\cdot) : W^{1,\tilde{p}}(D) \to W^{1,\tilde{p}}(D) \tag{38}$$

is invertible. Moreover,

$$\mu(x,k)|_D = [I + g_k * (q\cdot)]^{-1}1. \tag{39}$$

Proof. Use lemma 1.3 of [23] to decompose $g_k * (q\cdot)$ as $W^{1,\tilde{p}}(D) \xrightarrow{\iota} C(\overline{D}) \xrightarrow{q\cdot} L^p \xrightarrow{g_k*} W^{1,\tilde{p}} \to W^{1,\tilde{p}}(D)$, where ι is (compact) Sobolev imbedding and $1/p = 1/\tilde{p} + 1/2$. Thus (38) is Fredholm of index zero. To show that (38) is one-to-one, let $u \in W^{1,\tilde{p}}(D)$ satisfy

$$u + g_k * (qu) = 0 \qquad \text{in} \quad D. \tag{40}$$

Extend u to $\mathbb{R}^2$ by $u = -g_k * (qu) \in W^{1,\tilde{p}}$. Clearly, u satisfies $(-\Delta - 4ik\bar{\partial})u = -qu$, and by [23, lemma 1.5] we see that $u \equiv 0$ in $\mathbb{R}^2$. Finally, note the difference of the functions in (39) satisfies (40), so they must coincide and the theorem is proved. □

Here we will describe a projection method for solving μ as generally described in [18] and [19]. A detailed convergence proof is given in [24].

Given q as in the assumptions of theorem 4.2, let $d > 0$ be so large that $\operatorname{supp}(q) \subset D := \{x \in \mathbb{R}^2 \mid -d < x_i < d, i = 1,2\}$. For any $N \geqslant 2$, denote $h = 2d/(N-1)$ and define a finite grid $G_N \subset \overline{D}$ by

$$G_N := \{(x_1,x_2) \in \overline{D} | x_i = -d + \nu h, \nu = 0,\ldots,N-1, i = 1,2\}.$$

Let $x^{(j)}$, $j = 1,\ldots,N^2$, be a numbering of the points in G_N and define a linear subspace $V_N \subset W^{1,\tilde{p}}(D)$ by $V_N = \operatorname{span}\{v_j | j = 1,\ldots,N^2\}$, where the continuous, piecewise linear basis functions $v_j : D \to \mathbb{R}$ are defined by the requirements (i) $v_j(x^{(k)}) = \delta_{jk}$ for $j,k = 1,\ldots,N^2$; (ii) v_j is linear on all triangular subsets of D having vertices at grid points, two sides parallel to the coordinate axis and third side having slope 1.

Since $W^{1,\tilde{p}}(D)$ functions are continuous and bounded on $\overline{D}$ by Sobolev imbedding, we are able to define a continuous projection

$$P_N : W^{1,\tilde{p}}(D) \to V_N, \qquad P_N(f) = \sum_{j=1}^{N^2} f(x^{(j)})v_j(x).$$

With $k \in \mathbb{C} \setminus 0$ fixed, the projection method is as follows.

(1) Pick an initial $N \geqslant 2$.
(2) Compute the $N^2 \times N^2$ matrix $A_N = (a_N^{ij})$, where

$$a_N^{ij} := (g_k * (qv_j))(x^{(i)}) = \int_D g_k(x^{(i)} - y)q(y)v_j(y)\,\mathrm{d}y.$$

(3) If the matrix $P_N(I + A) = I + A_N$ is not invertible, go back to step 2 with a larger N. Otherwise go to step 4.
(4) Find approximate point values $\mu_N(x^{(j)},k)$ of $\mu(\cdot,k)$ at the grid points:

$$\begin{bmatrix} \mu_N(x^{(1)},k) \\ \vdots \\ \mu_N(x^{(N^2)},k) \end{bmatrix} = (I + A_N)^{-1} \begin{bmatrix} 1 \\ \vdots \\ 1 \end{bmatrix}.$$

5. The inverse problem

The inverse conductivity problem is known to be ill-posed. However, we note that the work of Nachman and Liu [20,23] yield a conditional stability result valid for conductivities satisfying an *a priori* estimate $1/M \leqslant \|\gamma\|_{W^{2,p}(\Omega)} \leqslant M$. The inversion step from $\boldsymbol{t}(k)$ to γ has linear stability whereas the step from Λ_γ to $\boldsymbol{t}(k)$ only has a logarithmic stability estimate.

In the following, let Ω be the unit disc.

5.1. From Λ_γ to $\boldsymbol{t}(k)$

Instead of solving equation (10) numerically we use the approximation $\psi(x,k)|_{\partial\Omega} \approx \mathrm{e}^{\mathrm{i}kx}$. This should be more accurate for small q. Expanding $\mathrm{e}^{\mathrm{i}kx}$ in a Fourier series on the circle $x = \mathrm{e}^{\mathrm{i}\theta}$ yields [14]

$$\mathrm{e}^{\mathrm{i}kx} = \sum_{n=-\infty}^{\infty} a_n(k)\mathrm{e}^{\mathrm{i}n\theta} \qquad \text{with} \quad a_n(k) = \begin{cases} \dfrac{(\mathrm{i}k)^n}{n!}, & n \geqslant 0 \\ 0, & n < 0. \end{cases}$$

Substituting this series into formula (11) gives

$$\boldsymbol{t}(k) \approx \sum_{n=1}^{\infty} (\lambda_n - |n|) \frac{(-1)^n |k|^{2n}}{(n!)^2}. \tag{41}$$

Note that the numerical method of section 4.1 gives the difference $\lambda_n - |n|$ explicitly.

We do not discuss the validity of this approximation. By theorem 4.1 of [23] we know that any function $\boldsymbol{t}(k)$ that satisfies $\boldsymbol{t}(k)/\bar{k} \in L^r$ for $2-\varepsilon < r < 2+\varepsilon$ is the scattering transform of a conductivity-type function. The application of this approximation gives reasonable results in our examples even when q is not small.

5.2. The solution of the $\bar{\partial}$ equation

To obtain the solution of the $\bar{\partial}$ equation (12), we solve the weakly singular Fredholm equation of the second kind

$$\mu(x, s^{(j)}) = 1 + \frac{1}{(2\pi)^2} \int_{\mathbb{R}^2} \frac{\boldsymbol{t}(k)}{(s^{(j)} - k)\bar{k}} e_{-x}(k) \overline{\mu(x,k)}\, \mathrm{d}k \tag{42}$$

for a suitable collection of $x \in \Omega$ and $s^{(j)} \in \mathbb{C} \setminus 0$, such that $s^{(j)} \to 0$ as $j \to \infty$. This will yield gamma as

$$\gamma^{1/2}(x) = \lim_{j\to\infty} \mu(x, s^{(j)}). \tag{43}$$

By [20] the $\bar{\partial}$ inversion $\boldsymbol{t} \to \gamma$ is well-posed and even contributes some smoothing. To solve the $\bar{\partial}$ equation numerically, we essentially apply the method of product integrals [1], which is an adaptation of the Nystrom method for second-order Fredholm integral equations. The idea is to factor the integrand into its smooth and singular parts, and approximate the smooth part with a simple function, such as an interpolatory polynomial. The new integrand is then computed analytically where possible. Here we adapt the 1D method presented in [1] to two dimensions.

For $s \in \mathbb{C} \setminus 0$ write equation (42) as

$$\mu(x,s) = 1 + \frac{1}{4\pi^2} \int_{\mathbb{R}^2} H(s,k) L(x,k) \overline{\mu(x,k)}\, \mathrm{d}k_1\, \mathrm{d}k_2$$

where $k = k_1 + ik_2$ and

$$H(s,k) := \frac{1}{(s-k)} \qquad \text{and} \qquad L(x,k) := \frac{\boldsymbol{t}(k)}{\bar{k}} e_{-x}(k).$$

Note from theorem 3.1 that $|\boldsymbol{t}(k)| \leqslant C|k|^2$ and hence $\boldsymbol{t}(k)/\bar{k}$ is bounded at $k = 0$. By theorem 3.2, we see that the integrand in (42) approaches zero as $|k| \to \infty$. Hence for numerical purposes we choose $A, C > 0$ sufficiently large, and instead solve

$$\mu(x,s) = 1 + \frac{1}{4\pi^2} \int_{-A}^{A} \int_{-C}^{C} H(s,k) L(x,k) \overline{\mu(x,k)} \, \mathrm{d}k_1 \, \mathrm{d}k_2.$$

Next, define a mesh on $[-A, A] \times [-C, C]$ in such a way that $k_1 = 0, k_2 = 0$ is not a mesh point. Let

$$u_j = -A + j h_u^j, \qquad j = 0, \ldots, N+1$$
$$v_i = -C + i h_v^i, \qquad i = 0, \ldots, N+1.$$

where $u_{j+1} - u_j = h_u^j > 0$, $j = 0, \ldots, N$ and $v_{i+1} - v_i = h_v^i > 0$, $i = 0, \ldots, N$.

Since $\mu \sim 1$ for $|k|$ large, on the set $S := \{[u_j, u_{j+1}] \times [v_i, v_{i+1}]: \ j \in \{0, N-1\}$ or $i \in \{0, N-1\}\}$ of outer mesh elements we set $\mu \equiv 1$. Then we wish to solve

$$\mu(x,s) = g(x,s) + \frac{1}{4\pi^2} \sum_{j=1}^{N-1} \sum_{i=1}^{N-1} \int_{u_j}^{u_{j+1}} \int_{v_i}^{v_{i+1}} H(s,k) L(x,k) \overline{\mu(x,k)} \, \mathrm{d}k_1 \, \mathrm{d}k_2 \tag{44}$$

where

$$g(x,s) := 1 + \frac{1}{4\pi^2} \int_S H(s,k) L(x,k) \, \mathrm{d}k_1 \, \mathrm{d}k_2. \tag{45}$$

We then approximate the function $f(x,k) := L(x,k)\overline{\mu(x,k)}$ by an interpolatory polynomial. Here, we use bilinear interpolation and introduce the notation

$$[f(x,k_1,k_2)]_{ji} := (1-t)(1-w) f_{j,i} + t(1-w) f_{j+1,i} + tw f_{j+1,i+1} + (1-t) w f_{j,i+1}$$

where $f_{j,i} := f(x, u_j, v_i)$, $t := \frac{k_1 - u_j}{h_u^j}$, and $w := \frac{k_2 - v_i}{h_v^i}$.

For $x \in \Omega$ define the numerical integration operator by

$$\kappa_N \mu(x,s) := \sum_{j=1}^{N-1} \sum_{i=1}^{N-1} \int_{u_j}^{u_{j+1}} \int_{v_i}^{v_{i+1}} H(s,k) [f(x,k_1,k_2)]_{ji} \, \mathrm{d}k_1 \, \mathrm{d}k_2. \tag{46}$$

To obtain a linear system, we choose s to be the nodes of the inner mesh elements $\{s = (u_j, v_i)\}_{j,i=1}^{N}$. Then to form $g(x,s)$ and $\kappa_N \mu(x,s)$ the following integrals must be evaluated for $j, i = 0, \ldots, N$ and $s = (u_m, v_n)$, $m, n = 1, \ldots, N$:

$$J_1^{ji}(s) := \int_{u_j}^{u_{j+1}} \int_{v_i}^{v_{i+1}} \frac{1}{(s-k)} \, \mathrm{d}k_1 \, \mathrm{d}k_2 \tag{47}$$

$$J_2^{ji}(s) := \int_{u_j}^{u_{j+1}} \int_{v_i}^{v_{i+1}} \frac{k_1}{(s-k)} \, \mathrm{d}k_1 \, \mathrm{d}k_2 \tag{48}$$

$$J_3^{ji}(s) := \int_{u_j}^{u_{j+1}} \int_{v_i}^{v_{i+1}} \frac{k_2}{(s-k)} \, \mathrm{d}k_1 \, \mathrm{d}k_2 \tag{49}$$

$$J_4^{ji}(s) := \int_{u_j}^{u_{j+1}} \int_{v_i}^{v_{i+1}} \frac{k_1 k_2}{(s-k)} \, \mathrm{d}k_1 \, \mathrm{d}k_2. \tag{50}$$

Note that when s lies on a corner of the mesh element over which we are integrating, an integrable singularity will be present in the integrand. When s does not coincide with a corner

of the mesh element over which we are integrating, the above integrals are not singular, and they can be computed using a numerical quadrature method such as 2D Gauss–Legendre quadrature.

The integrals over mesh elements on which s is a corner can be evaluated analytically. Suppose $s = (u_j, v_i)$. Then, for a uniform mesh $h_u^j = h_v^i = h$ we have

$$J_1^{ji}(u_j, v_i) = -\frac{h}{2}\left(1 - \sqrt{-1}\right)\left(\frac{\pi}{2} + \log 2\right) \tag{51}$$

$$J_2^{ji}(u_j, v_i) = I_2 + u_j J_1^{ji}(u_j, v_i); \qquad I_2 = -\frac{h^2}{2}\left(1 - \sqrt{-1}\log 2\right) \tag{52}$$

$$J_3^{ji}(u_j, v_i) = I_3 + v_i J_1^{ji}(u_j, v_i); \qquad I_3 = -\frac{h^2}{2}\left(\log 2 - \sqrt{-1}\right) \tag{53}$$

$$J_4^{ji}(u_j, v_i) = h^3\left(1 - \sqrt{-1}\right)\left(\frac{\pi - 4}{12} - \frac{1}{6}\log 2\right) + v_i I_2 + u_j I_3 + u_j v_i J_1^{ji}(u_j, v_i). \tag{54}$$

The other 12 cases in which s lies on one of the other three corners of the mesh element are very similar, and the case of a nonuniform mesh is omitted for brevity.

Denote $\mu_{ji}(x) := \mu(x, (u_j, v_i))$. By regrouping terms, the numerical integration operator in (46) can now be written as

$$\kappa_N \mu(x, s) = \sum_{j=1}^{N-1}\sum_{i=1}^{N-1} A^{ji}(x)\overline{\mu_{ji}(x)} \tag{55}$$

where

$$A^{ji}(x) = a_{ji}(x)J_1^{ji}(s) + b_{ji}(x)J_2^{ji}(s) + c_{ji}(x)J_3^{ji}(s) + d_{ji}(x)J_4^{ji}(s). \tag{56}$$

Now choose $\{s = (u_k, v_l)\}_{k,l=1}^N$ and define an N^2 by N^2 matrix $\boldsymbol{A}(x) = (A^{ji}(x))$, where $A^{ji}(x)$ is the linear combination of the $J_\alpha^{ji}((u_k, v_l))$ above, $\alpha \in \{\overline{1, 4}\}$. This results in the linear system

$$\boldsymbol{I}\boldsymbol{\mu}(x) - \boldsymbol{A}\bar{\boldsymbol{\mu}}(x) = \boldsymbol{g}(x) \tag{57}$$

where $\boldsymbol{I}$ is the $N^2 \times N^2$ identity matrix. This system can be solved by equating the real and imaginary parts to obtain two linear systems in real variables with two vectors of unknowns. Namely,

$$(\boldsymbol{I} - \mathrm{Re}\,(\boldsymbol{A}))\boldsymbol{a} - \mathrm{Im}\,(\boldsymbol{A})\boldsymbol{b} = \mathrm{Re}\,(\boldsymbol{g}) \tag{58}$$

$$(\boldsymbol{I} + \mathrm{Re}\,(\boldsymbol{A}))\boldsymbol{b} - \mathrm{Im}\,(\boldsymbol{A})\boldsymbol{a} = \mathrm{Im}\,(\boldsymbol{g}) \tag{59}$$

where $\boldsymbol{\mu} = \boldsymbol{a} + \mathrm{i}\boldsymbol{b}$. Solving the linear system gives $\{\mu(x, (u_j, v_i))\}_{j,i=1}^N$.

Note that this procedure must be repeated for each x in the region of interest. However, the factors $J_\alpha^{ji}(s)$ in the matrix $\boldsymbol{A}$ need only be computed once, which saves computation time.

6. Numerical examples

In this section we present reconstructions of high-contrast and low-contrast C^∞ conductivities from numerically simulated Dirichlet-to-Neumann data. We include two radially symmetric conductivities. By theorem 3.3 we know that for a radial conductivity, the scattering transform $\boldsymbol{t}(k)$ is rotationally invariant and real-valued. Thus it is enough to find $\boldsymbol{t}(k)$ for a collection of positive real numbers instead of a 2D grid of k-values.

The method of section 4.3 was used with $D = [-\frac{1}{2}, \frac{1}{2}]^2$ and $N = 29$ to solve the forward problem of computing $\mu(x, k)$ from knowledge of γ. This enabled us to compute $\boldsymbol{t}(k)$ directly from (6) using Gauss–Legendre quadrature for purposes of comparison with the $\boldsymbol{t}(k)$

computed from the Dirichlet-to-Neumann data. The Dirichlet-to-Neumann data was obtained by the method described in section 4.1, using roughly $N = 9000$. The scattering transform $\boldsymbol{t}(k)$ was computed from the data using the method described in section 5.1. The functions μ were reconstructed from $\boldsymbol{t}(k)$ by the method described in section 5.2.

We start by constructing a building block for smooth conductivities. Let $0 < d < 1$ and define a non-negative function $\Psi_d \in C_0^\infty(\mathbb{R})$ by

$$\Psi_d(t) = \begin{cases} \mathrm{e}^{-\frac{2(d^2+t^2)}{(t+d)^2(t-d)^2}} & \text{for} \quad -d \leqslant t \leqslant d, \\ 0 & \text{otherwise.} \end{cases}$$

Define a radially symmetric function $\gamma \in C^\infty(\mathbb{R}^2)$ by

$$\gamma(r) := (\alpha \Psi_d(r) + 1)^2, \tag{60}$$

where $\alpha > -\exp(2/d^2)$ is a real constant. Note that $\operatorname{supp}(\gamma - 1) = \overline{B(0, d)}$ and that γ is bounded away from zero. The Schrödinger potential q, corresponding to γ, is now

$$q(r) = \frac{\Delta \gamma^{1/2}(r)}{\gamma^{1/2}(r)} = \frac{\Delta \Psi_d(r)}{\Psi_d(r) + 1/\alpha}, \tag{61}$$

and this expression is possible to compute in closed form.

6.1. Example 1

We begin by studying a radially symmetric, low-contrast conductivity in which a linearized reconstruction algorithm might also be expected to yield a good reconstruction. Let γ be given by (60) with $d = \frac{1}{2}$ and $\alpha = (\sqrt{6/5} - 1)\mathrm{e}^8$. Then the conductivity γ has amplitude 1.2 and is very near one for $|x| > 0.2$. See figure 1 for a plot of $\gamma(x)$.

The Dirichlet-to-Neumann data $\lambda_n - |n|$, where λ_n are eigenvalues of Λ_γ, were computed for $n = 1, \ldots, 32$ by the method given in section 4.1, with $N = 9000$. Figure 4 contains logarithmic plots of the upper and lower bounds for $\{\lambda_n - |n|\}_{n=1}^{32}$.

The scattering transform $\boldsymbol{t}_{\mathrm{dat}}(k)$ was computed from the lower-bound data $\{\lambda_n - |n|\}_{n=1}^{32}$ using the series (41). In figure 3 we compare the reconstructed scattering transform $\boldsymbol{t}_{\mathrm{dat}}(k)$ with $\boldsymbol{t}_{LS}(k)$ obtained from the solution of the Lippmann–Schwinger equation as described above and to the Fourier transform $\hat{q}$ evaluated at $2|k|$. It is seen that the series (41) begins to diverge around $k = 50$. However, in this example, $\boldsymbol{t}_{\mathrm{dat}}(k)$ is in close agreement with $\boldsymbol{t}_{LS}(k)$, with a relative error of $\frac{\|\boldsymbol{t}_{LS}(k) - \boldsymbol{t}_{\mathrm{dat}}(k)\|_\infty}{\|\boldsymbol{t}_{LS}(k)\|_\infty} < 2\%$ for $k \in [1, 35]$.

Plots of the functions $\mu(x, k)$ computed from the Lippmann–Schwinger equation are found in figure 2. To obtain reconstructions of γ, the $\bar{\partial}$ equation was solved using the method presented in section 5.2 with $\boldsymbol{t}_{\mathrm{dat}}(k)$ and $\boldsymbol{t}_{LS}(k)$. Equation (42) was solved on a uniform k mesh with $h = 1.8$ and $A = C = 35$. It was solved for the x values $-0.25, -0.2, \ldots, 0.2, 0.25$. Note that for this k mesh, the mesh points nearest the origin satisfy $|k_1| = 0.9$, $|k_2| = 0.9$. The value of $\gamma^{1/2}(x)$ was simply approximated by $\gamma^{1/2}(x) := \operatorname{Re}(\mu(x, (0.9, 0.9)))$. The reconstructions of γ are found in figures 5 and 6. The relative errors $\frac{\|\gamma_{\mathrm{app}} - \gamma\|_\infty}{\|\gamma\|_\infty}$ were found to be 1% for both the reconstruction from $\boldsymbol{t}_{LS}(k)$ and the reconstruction from $\boldsymbol{t}_{\mathrm{dat}}(k)$.

6.2. Example 2

In this example we consider a radially symmetric high-contrast conductivity in which we would not expect a linearized reconstruction algorithm to give accurate conductivity values. We let γ be given by (60) with $d = \frac{1}{2}$ and $\alpha = \mathrm{e}^8$. The conductivity is plotted in figure 1 and has amplitude 4 and is very near one for $|x| > 0.2$.

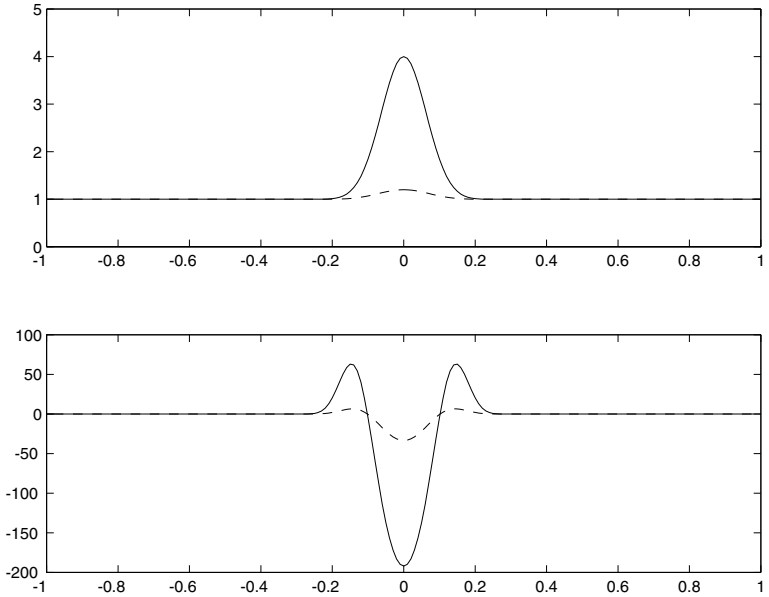

Figure 1. Upper plot: profiles of the conductivities $\gamma(x)$ for the low-contrast conductivity of example 1 (dashed curve) and the high-contrast conductivity of example 2 (solid curve). Lower plot: the corresponding potentials $q(x)$ of example 1 (dashed curve) and example 2 (solid curve).

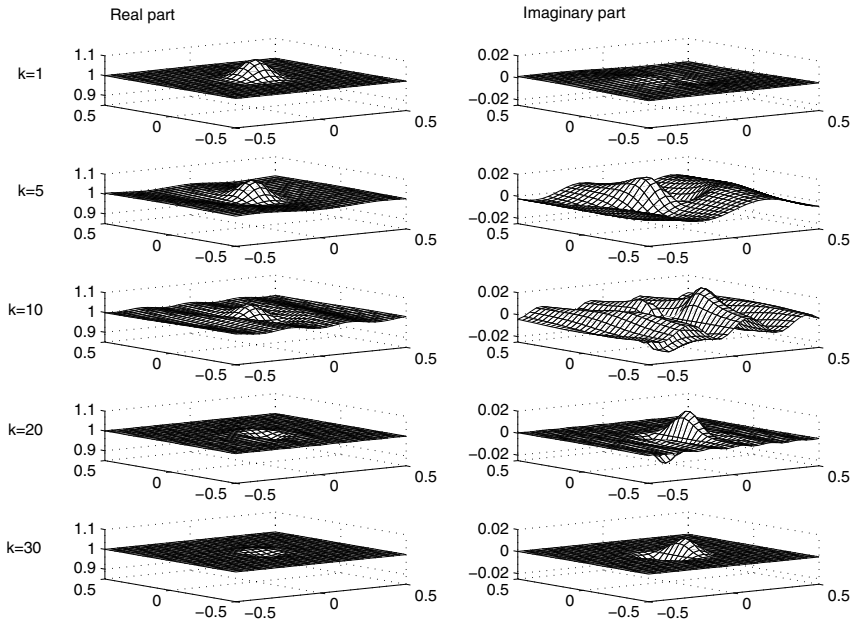

Figure 2. The real and imaginary parts of the functions $\mu(x, k)$ of example 1 for k values 1, 5, 10, 20 and 30. Here x ranges in the square $D = [-\frac{1}{2}, \frac{1}{2}]^2$.

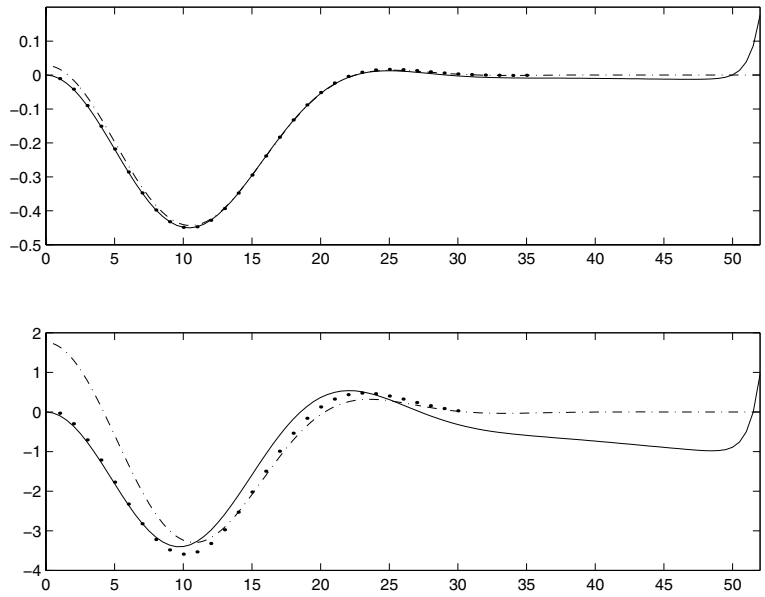

Figure 3. The Fourier transforms $\hat{q}(2|k|)$ of example 1 (upper plot) and example 2 (lower plot) are presented as dot-dashed curves. Solid curves represent the approximate scattering transforms $\boldsymbol{t}_{\text{dat}}(k)$ decribed in section 5.1. Dots represent values of $\boldsymbol{t}_{LS}(k)$ computed with the direct solver presented in section 4.3.

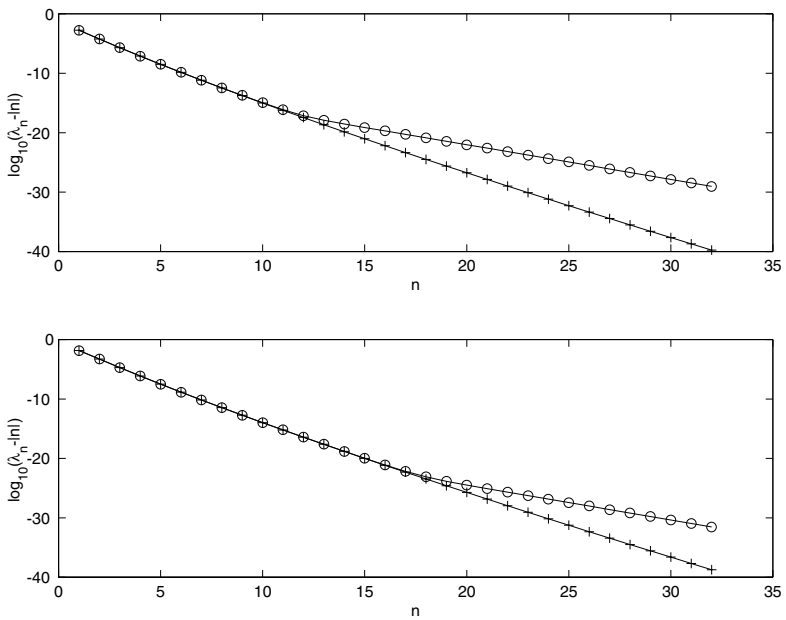

Figure 4. Logarithmic plots of the upper (o) and lower (+) bounds for $\{\lambda_n - |n|\}_{n=1}^{32}$ for example 1 (upper plot) and example 2 (lower plot).

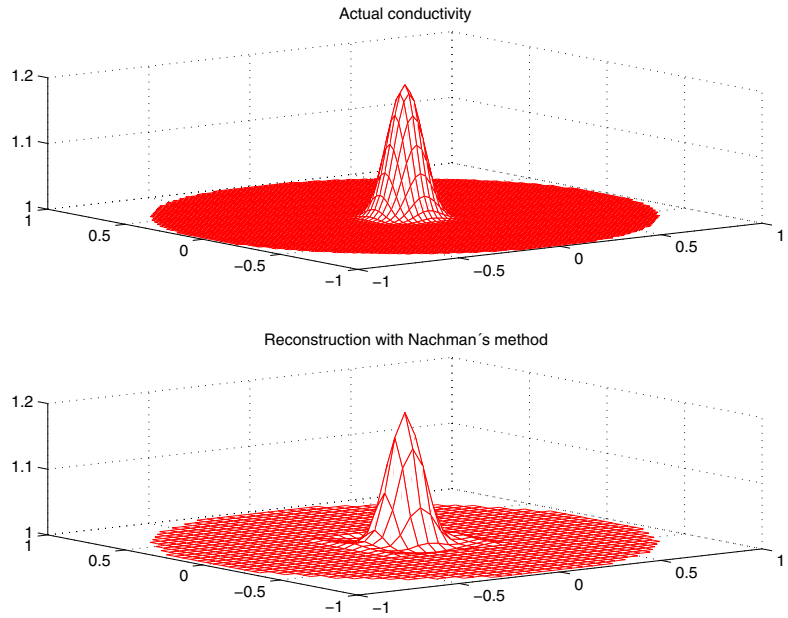

Figure 5. Upper plot: conductivity of example 1. Lower plot: reconstruction from $\boldsymbol{t}_{\mathrm{dat}}(k)$.

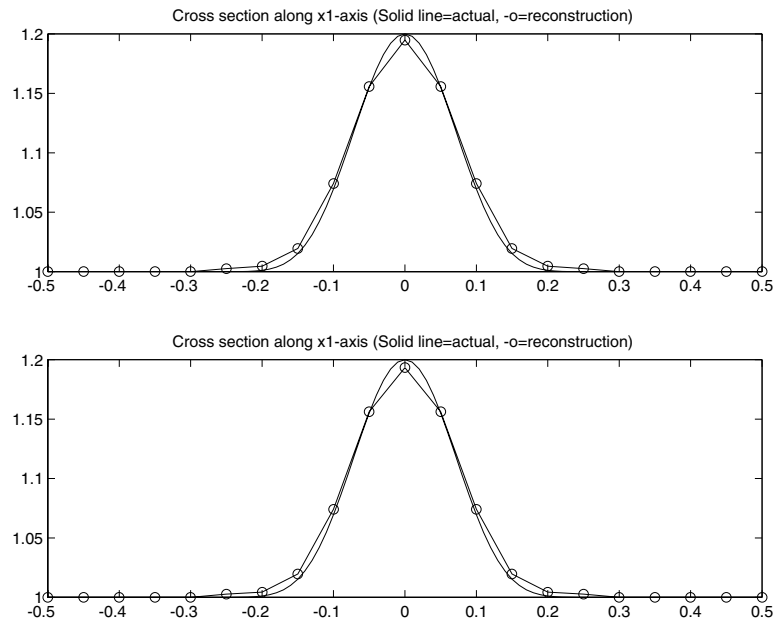

Figure 6. Upper plot: comparison of the actual conductivity γ and the reconstruction from $\boldsymbol{t}_{LS}(k)$ for example 1. Lower plot: comparison of the actual conductivity and the reconstruction from $\boldsymbol{t}_{\mathrm{dat}}(k)$.

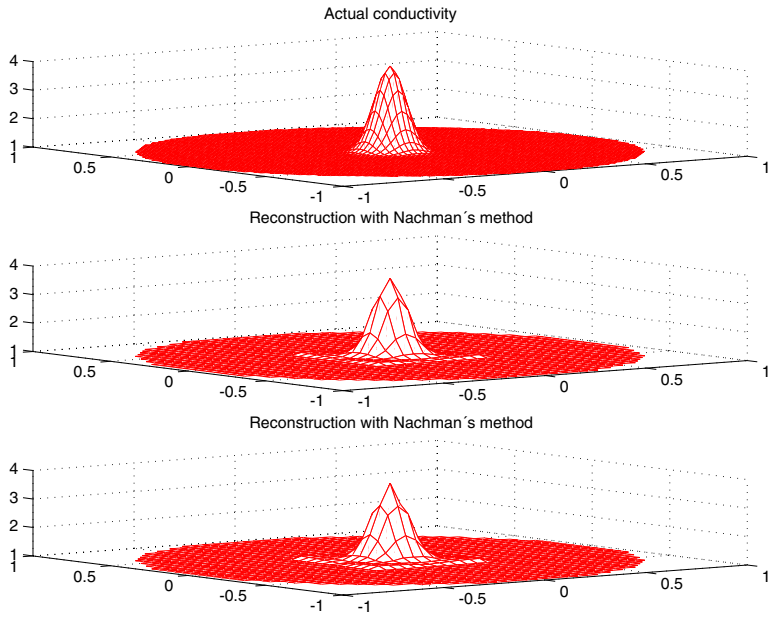

Figure 7. Upper plot: conductivity of example 2. Centre plot: reconstruction from $t_{LS}(k)$. Lower plot: reconstruction from $t_{\mathrm{dat}}(k)$.

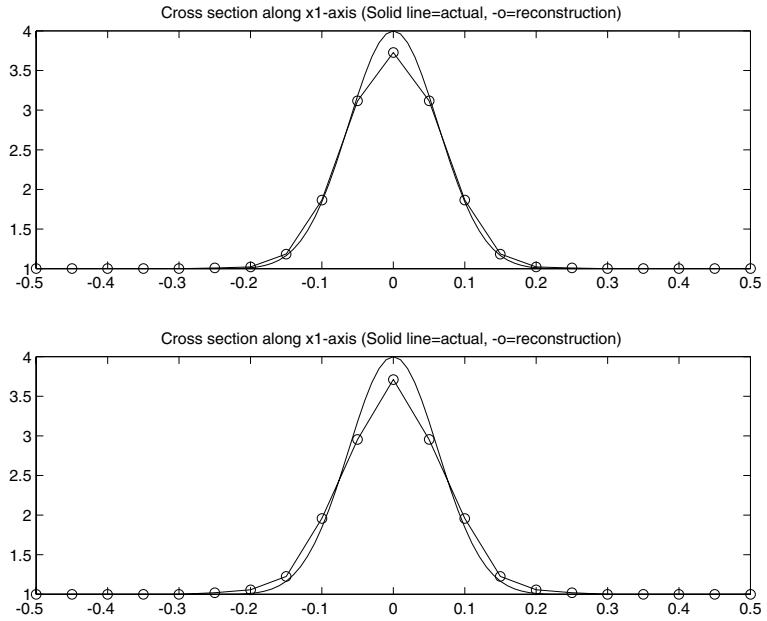

Figure 8. Upper plot: comparison of the actual conductivity γ and the reconstruction from $t_{LS}(k)$ for example 2. Lower plot: comparison of the actual conductivity and the reconstruction from $t_{\mathrm{dat}}(k)$.

Figure 4 contains logarithmic plots of the upper and lower bounds for $\{\lambda_n - |n|\}_{n=1}^{32}$. Again the scattering transform $\boldsymbol{t}_{\text{dat}}(k)$ was computed from the lower-bound data. Plots of $\boldsymbol{t}_{\text{dat}}(k)$, $\boldsymbol{t}_{LS}(k)$, and $\hat{q}(2|k|)$ are found in figure 3. In this example $\boldsymbol{t}_{\text{dat}}(k)$ and $\boldsymbol{t}_{LS}(k)$ differ more significantly from $\hat{q}(2|k|)$, and the relative error between $\boldsymbol{t}_{\text{dat}}(k)$ and $\boldsymbol{t}_{LS}(k)$ is 15% for $k \in [1, 35]$. Note that $\boldsymbol{t}_{\text{dat}}(k)$ fails to approach zero for large $|k|$. Despite this fact, $\boldsymbol{t}_{\text{dat}}(k)$ gave very good reconstructions of γ. The $\bar{\partial}$ equation was solved with the same k mesh and x values as in example 1. Again, the values of $\gamma^{1/2}(x)$ were simply approximated by $\gamma^{1/2}(x) := \text{Re}\,(\mu(x, (0.9, 0.9)))$. The reconstructions of γ are found in figures 7 and 8. The relative errors in γ were found to be 6.8% for the reconstruction from $\boldsymbol{t}_{LS}(k)$ and 7.2% for the reconstruction from $\boldsymbol{t}_{\text{dat}}(k)$.

7. Conclusion

The purpose of this paper was to demonstrate the feasibility of implementing the direct reconstruction algorithm outlined by Nachman in [23]. We described our implementation and several relevant theoretical results. We do not give a thorough study of the error and computational complexity specific to our implementation. The method was found to effectively restore conductivity values for both high- and low-contrast radially symmetric C^∞ conductivities.

The method applies to more general conductivities and, in particular, the solution of the $\bar{\partial}$ equation took no advantage of the rotational symmetry.

Acknowledgments

The authors thank A Nachman for helpful discussions. The authors also acknowledge the NSF for supporting JM under an NSF Mathematical Sciences Postdoctoral Fellowship and the Helsinki University of Technology for hospitality and travel support for JM; the Finnish Ministry of Education, Finnish Academy of Science and Letters, the Emil Aaltonen Foundation, the Instrumentarium Science Foundation and the Finnish Cultural Foundation for the support of SS. The numerical calculations in this paper were performed using computing equipment supported in part by NSF grant DMS 9872019.

References

[1] Atkinson K 1989 *An Introduction to Numerical Analysis* 2nd edn (New York: Wiley)
[2] Blue R 1997 Real-time three-dimensional electrical impedance tomography *PhD Thesis* (RPI, Troy, NY)
[3] Boiti M, Leon J P, Manna M and Pempinelli F 1987 On a spectral transform of a KdV-like equation related to the Schrödinger operator in the plane *Inverse Problems* **3** 25–36
[4] Borcea L, Berryman J G and Papanicolaou G C 1996 High-contrast impedance tomography *Inverse Problems* **12** 835–58
[5] Borcea L, Berryman J G and Papanicolaou G C 1999 Matching pursuit for imaging high-contrast impedance tomography *Inverse Problems* **15** 811–49
[6] Brown R M and Uhlmann G 1997 Uniqueness in the inverse conductivity problem for nonsmooth conductivities in two dimensions *Commun. Partial Diff. Eqns* **22** 1009–27
[7] Calderon A P 1980 On an inverse boundary value problem. *Seminar on Numerical Analysis and its Applications to Continuum Physics* (Society Brasileira de Matemàtica) pp 65–73
[8] Cheney M and Isaacson D 1995 Issues in electrical impedance imaging *IEEE Comput. Sci. Eng.* **2** 53–62
[9] Cheney M, Isaacson D and Newell J C 1999 Electrical impedance tomography *SIAM Rev.* **41** 85–101
[10] Colton D and Kress R 1983 *Integral Equation Methods in Scattering Theory* (New York: Wiley)
[11] Faddeev L D 1966 Increasing solutions of the Schrödinger equation *Sov.–Phys. Dokl.* **10** 1033–5
[12] Gilbarg D and Trudinger N S 1977 *Elliptic Partial Differential Equations of Second Order* (Berlin: Springer)

[13] Gisser D G, Isaacson D and Newell J C 1990 Electric current tomography and eigenvalues *SIAM J. Appl. Math.* **50** 1623–34
[14] Isaacson D and Cheney M 1991 Effects of measurement precision and finite numbers of electrodes on linear impedance imaging algorithms *SIAM J. Appl. Math.* **15** 1705–31
[15] Isakov V 1998 *Inverse Problems for Partial Differential Equations* (Berlin: Springer)
[16] Knowles I 1998 A variational algorithm for electrical impedance tomography *Inverse Problems* **14** 1513–25
[17] Kohn R V and Vogelius M 1985 Determining conductivity by boundary measurements II. Interior results *Commun. Pure Appl. Math.* **38** 643–67
[18] Krasnosel'skii M A, Vainikko G M, Zabreiko P P, Rutitskii Ya B and Stetsenko V Ya 1972 *Approximate Solution of Operator Equations* (Groningen: Wolters-Noordhoff)
[19] Kress R 1989 *Linear Integral Equations* (Berlin: Springer)
[20] Liu L 1997 Stability estimates for the two-dimensional inverse conductivity problem *PhD Thesis* University of Rochester
[21] Mueller J L, Isaacson D and Newell J C 1999 A reconstruction algorithm for electrical impedance tomography data collected on rectangular electrode arrays *IEEE Trans. Biomed. Eng.* **49** at press
[22] Nachman A I 1988 Reconstructions from boundary measurements. *Ann. Math.* **128** 531–76
[23] Nachman A I 1996 Global uniqueness for a two-dimensional inverse boundary value problem *Ann. Math.* **143** 71–96
[24] Siltanen S 1999 Electrical impedance tomography and Faddeev Green functions *PhD Thesis* Helsinki University of Technology
[25] Sylvester J 1992 A convergent layer stripping algorithm for the radially symmetric impedance tomography problem *Commun. Partial Diff. Eqns* **17** 1955–94
[26] Sylvester J and Uhlmann G 1987 A global uniqueness theorem for an inverse boundary value problem *Ann. Math.* **125** 153–69
[27] Sylvester J and Uhlmann G 1990 The Dirichlet to Neumann map and applications *Inverse Problems in Partial Differential Equations* (Philadelphia: SIAM)
[28] Yorkey T J, Webster J G and Tompkins W J 1987 Comparing reconstruction algorithms for electrical impedance tomography *IEEE Trans. Biomed. Eng.* **34** 843–52